

Facile synthesis of $\text{Cu}_2\text{FeSnS}_4$ nanoparticles for solar cell applications

M. CAO^{a*}, B. L. ZHANG^a, C. LI^a, J. HUANG^a, Y. SUN^b, L. J. WANG^a, Y. SHEN^{a*}

^a*School of materials Science and Engineering, Shanghai University, Shanghai 200072, China*

^b*National Laboratory for Infrared Physics, Shanghai Institute of Technical Physics, Chinese Academy of Sciences, Shanghai 200083, China*

$\text{Cu}_2\text{FeSnS}_4$ (CFTS) nanoparticles have been synthesized by solvothermal method and their structural and photovoltaic properties have been studied. The bandgaps of the as-synthesized particles are about 1.56 ~ 1.67 eV determined by UV-Vis absorption spectra. The average grain sizes of CFTS nanoparticles increase with increasing the reaction temperatures and times, while decrease with increasing the amounts of Ethylenediamine (En). CFTS nanosheets will form at longer reaction times and higher reaction temperatures. The photovoltaic properties have been investigated with CFTS nanoparticle-sensitized solar cells, and the power conversion efficiencies are found to increase with decreasing the average sizes of the nanoparticles.

(Received August 30, 2014; accepted June 09, 2016)

Keywords: Crystal growth, Solvothermal, Semiconductors, Optical properties

1. Introduction

Recently, solar cells have attracted substantial interests owing to the energy crisis and serious environmental pollution. Although silicon based solar cells have been commercially produced, their prices remain high, and their power conversion efficiencies are difficult to be enhanced further. As such, recent research has partially focused on CdTe [1-3] and $\text{CuIn}_{(1-x)}\text{Ga}_x\text{Se}_2$ (CIGS) [4-6] based solar cells. And CdTe solar panels have been mass-produced for years. However, cadmium is toxic element and indium is rare and expensive element. Therefore, cost-effective, non-toxic and earth-abundant photovoltaic materials are of considerable interests, including $\text{Cu}_2\text{ZnSnS}_4$ (CZTS) [7,8] and $\text{Cu}_2\text{FeSnS}_4$ (CFTS) [9], which have direct band gaps of about 1.5 eV and high optical absorption coefficients (over 10^4 cm^{-1}) in the UV-Visible range. As to mention is that, CZTS and CFTS nanocrystals have caused great attention due to their high throughput, efficient materials usage and suitability for large-area production [10]. These nearly monodisperse CZTS and CFTS nanocrystals with cation disordered zinc-blende and wurtzite structures are usually synthesized by hot-injection method [9,11].

High-quality CZTS and CFTS nanocrystals can be synthesized facily by the solvothermal method [12,13], which make us very easy to control the structural, morphological and optical properties of CFTS nanoparticles. Beside their excellent performances in thin film solar cells, their applications in dye sensitized solar cells (DSSCs) have also been widely investigated [14,15]. The simple structures of DSSCs make it convenient for us to investigate the effect of the structural, morphological and optical properties of CFTS nanoparticles on their photovoltaic properties. In this paper, we reported the synthesis of CFTS nanoparticles by a convenient solvothermal method. In this approach, Ethylenediamine (En) was added into a sealed autoclave and used as the solvent and reaction medium. The structural, morphological and optical properties of CFTS nanoparticles influenced by the amounts of En, reaction temperatures and times were investigated. The photovoltaic properties were examined with CFTS nanoparticle-sensitized solar cells.

2. Experiments

2.1 Materials

Copper (II) acetate monohydrate ($\text{Cu}(\text{CH}_3\text{COO})_2 \cdot \text{H}_2\text{O}$) (98 %), tin (IV) chloride pentahydrate ($\text{SnCl}_4 \cdot 5\text{H}_2\text{O}$) (98 %), iron (II) chloride anhydrous (FeCl_2) (98 %), and sulfur powder (99.999 %) were all of analytical grade and purchased from Strem Chemicals. Ethylenediamine (En) was analytical grade and all water used was deionized water.

2.2 Preparation of the CFTS nanoparticles

All solvothermal reactions were performed in a Teflon-lined reactor with the maximum volume of 50 ml. In a typical procedure, $\text{Cu}(\text{CH}_3\text{COO})_2 \cdot \text{H}_2\text{O}$ (0.8 ~ 1 mmol), FeCl_2 (0.9 ~ 1.1 mmol), $\text{SnCl}_4 \cdot 5\text{H}_2\text{O}$ (0.9 ~ 1.1 mmol), sulfur powder (2 ~ 2.2 mmol) were dissolved in 8 ~ 19 ml En under magnetic stirring in a beaker. The mixture was then loaded into the Teflon-lined stainless steel autoclave. The autoclave was sealed and maintained at 180 ~ 220 °C for 15 ~ 35 h and then cooled down to room temperature naturally. The precipitates were centrifuged and washed with ethanol and acetone, respectively. The final products were dispersed in ethanol.

2.3 Fabrication of CFTS nanoparticle-sensitized solar cells

A 100 nm-thick Pt layer and a 10 μm -thick TiO_2 on FTO glasses were used as photocathode and photoanode of CFTS nanoparticle-sensitized solar cells, respectively. The effective area of the solar cell was 0.25 cm^2 . At room temperature, the TiO_2 photoanode was immersed overnight in the ethanol solution which contained CFTS nanoparticles (0.5 mM). The polysulfide electrolyte, which consisted of 0.5 M Na_2S , 2.0 M S and 0.2 M KCl in the mixed solvent of water/methanol (3:7 by volume), were finally introduced between the electrodes by capillary force.

2.4 Characterizations

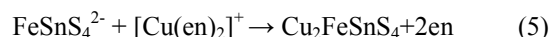
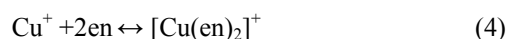
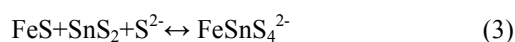
The structural properties of CFTS nanoparticles coated on quartz substrates were characterized by a Rigaku D/max 220 kV X-ray diffractometer (XRD, Cu-K α : $\lambda = 0.154$ nm). Morphological properties were investigated by using a JEM 2010-F transmission electron microscopy (TEM) and a Philips S360 scanning electron microscope (SEM), respectively. The elemental compositions of CFTS

nanoparticles were obtained using the energy dispersive X-ray spectroscopy (EDS). The absorption spectra of the as-synthesized CFTS nanoparticles dispersed in ethanol were measured using the Jasco UV-570 spectrophotometer in the wavelength range of 300-1500 nm at room temperature. A 514.5-nm line of He-Cd laser was used as the excitation source (JY-HR800) to measure the Raman spectra.

3. Results and discussion

3.1 Synthesis of CFTS nanoparticles

En molecules act both as a chelating agent and as a surface-passivating agent during the synthesis of CFTS nanoparticles [16]. Resulting from the nucleophilic attack, S atoms are firstly reduced to negatively charged S^{2-} ions. At the same time, Cu^{2+} ions are also reduced to Cu^+ ions by En because of the electron-transfer reaction. S^{2-} ions react with En chelated Cu^+ , Fe^{2+} , Sn^{4+} ions to form CFTS molecules. The reaction process can be described as the following equations:



The average compositions of the as-synthesized CFTS nanoparticles were determined by EDS, as shown in Fig. 1. The atomic percents of Cu, Fe, Sn and S increase with increasing the concentrations of $\text{Cu}(\text{CH}_3\text{COO})_2 \cdot \text{H}_2\text{O}$, FeCl_2 , $\text{SnCl}_4 \cdot 5\text{H}_2\text{O}$ and sulfur powder, respectively. The amounts of En influence little to the composition of CFTS nanoparticles. Then, 0.047 M $\text{Cu}(\text{CH}_3\text{COO})_2 \cdot \text{H}_2\text{O}$, 0.055 M FeCl_2 , 0.05 M $\text{SnCl}_4 \cdot 5\text{H}_2\text{O}$ and 0.111 M sulfur powder are most suitable to synthesize CFTS nanoparticles, whose composition ratios approach the theoretical value of 2:1:1:4 and exhibit a slight deficiency of Cu and richness of S. The deviations of the chemical compositions among the three metal elements are mainly due to different activities of the metal ions [17,18].

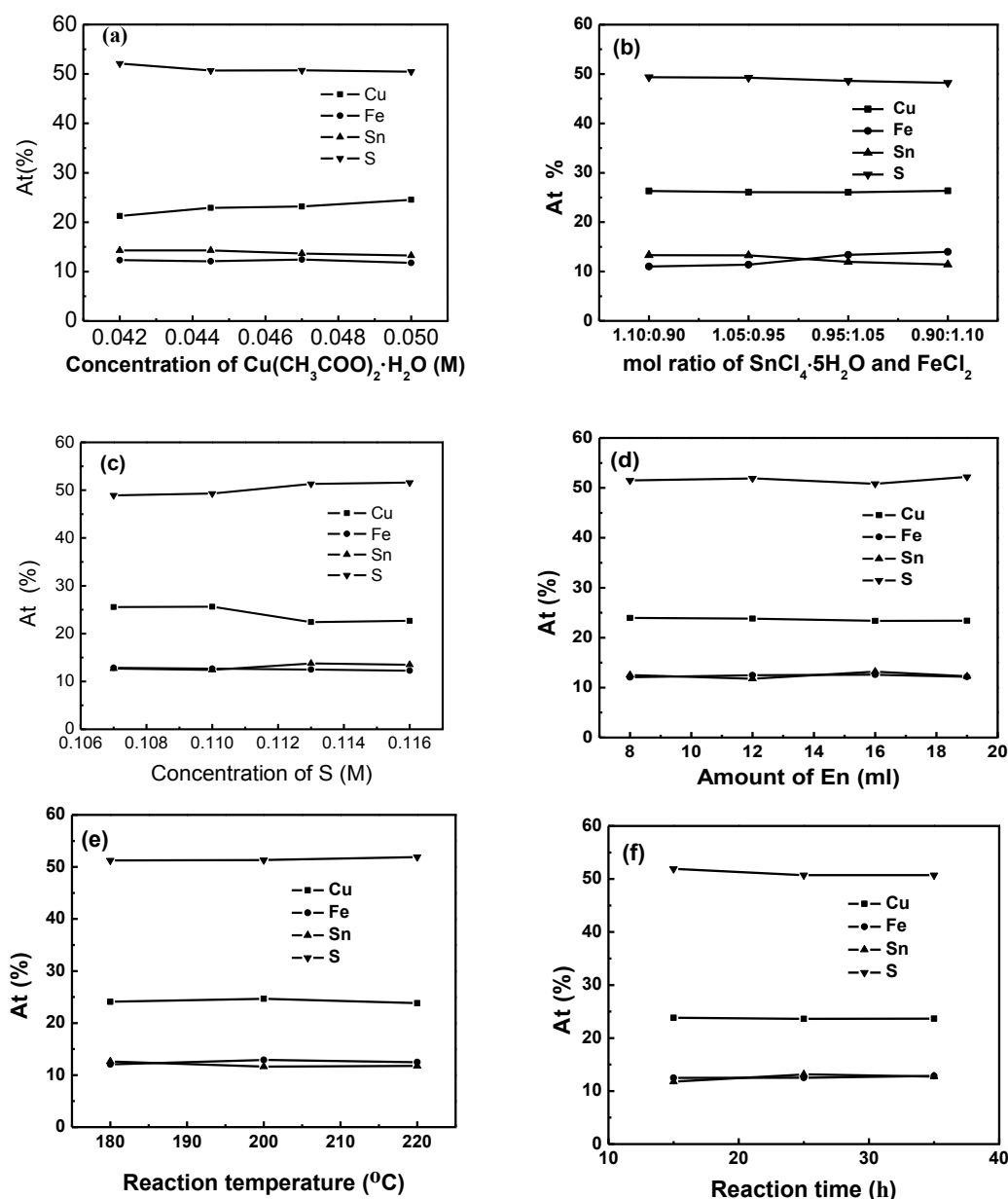


Fig. 1. Atomic percent of CFTS nanoparticles synthesized with different conditions: (a) concentration of $\text{Cu}(\text{CH}_3\text{COO})_2 \cdot \text{H}_2\text{O}$, (b) mol ratios of $\text{SnCl}_4 \cdot 5\text{H}_2\text{O}$ and FeCl_2 , (c) concentration of S, (d) amount of En, (e) temperatures and (f) times. The amount of En is 19 ml except condition (d).

It is well known that both CFTS and CZTS are tetrahedrally coordinated semiconductors in which each sulfur anion is bonded to four cations and each cation is bonded to four sulfur anions. Along the crystallographic c -direction, stannite CFTS has alternate cation and anion layers, i.e., $\text{CuCu}/\text{SS}/\text{FeSn}/\text{SS}$ [19,20]. The crystal structures of CFTS nanoparticles synthesized with different amounts of En, reaction temperatures and reaction times were characterized by XRD, as shown in Fig.2. In the XRD patterns, peaks at $2\theta = 28.5, 32.9, 47.2, 56.0, 59.0, 68.9, 76.7$ and 87.9° correspond to (112), (200), (220), (312), (224), (400), (316) and (424) planes of stannite CFTS (PDF 44-1476). Based on Scherrer's formula [21], the average grain sizes of CFTS nanoparticles were calculated to be

about 20 ~ 40 nm, as listed in Table 1. It indicates that the grain sizes decrease with increasing the amount of En, but increase with increasing the reaction temperatures and times. The values of lattice constants a ($a = b$) and c , which were calculated by using interplanar spacing formula and Bragg Equation, agree well with those of bulk CFTS. Small diffraction peaks at 26.9 and 31.5° correspond to (210) plane of SnS (PDF 65-2610) and (003) plane of FeS (PDF 65-9124), respectively, which indicate the existence of these secondary phases in the samples synthesized at 180 and 200 $^\circ\text{C}$. No obvious secondary phases could be found when the synthesis temperature is 220 $^\circ\text{C}$. However, the XRD pattern of CFTS also matches well with that of Cu_2SnS_3 (JCPDS 27-0198) and FeS (JCPDS 23-1123).

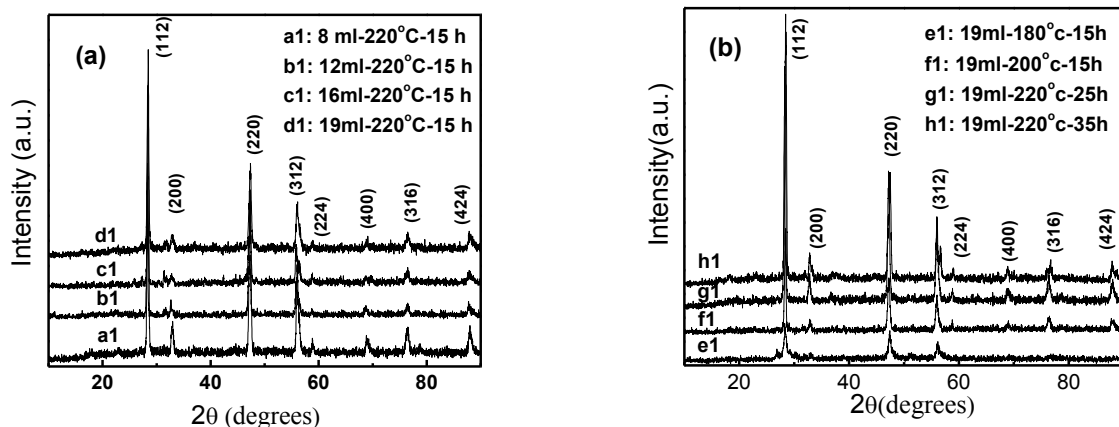


Fig. 2. The XRD patterns of CFTS nanoparticles. (a): CFTS nanoparticles synthesized with 9 (a₁), 12 (b₁), 16 (c₁) and 19 ml (d₁) En at 220 °C for 15 hours. (b) CFTS nanoparticles synthesized at 180 (e₁), 200 °C (f₁) with 19 ml En for 15 hours, and with 19 ml En at 220 °C for 25 (g₁) and 35 (h₁) hours.

Table 1. Physical parameters of as-synthesized CFTS nanoparticles.

Samples	FWHM	Grain size (nm)	a (a=b)	c	band-gap (eV)
220°C-15h -8ml	0.2	45	5.416	10.900	1.61
220°C-15h -12ml	0.207	43.2	5.524	10.687	1.60
220°C-15h -16ml	0.241	37.1	5.510	10.710	1.58
220°C-15h- 19ml	0.255	35.1	5.483	10.728	1.56
220°C-25h-19ml	0.245	36.8	5.424	10.893	1.64
220°C-35h-19ml	0.235	38.7	5.470	10.711	1.67
200°C-15h-19ml	0.327	27.4	5.485	10.807	1.62
180°C-15h-19ml	0.350	25.8	5.548	10.598	1.63

To identify the phase purity of CFTS nanoparticles synthesized at 220 °C using different amounts of En, Raman characterizations were carried out, as shown in Fig.3. The existence of tetragonal CFTS is identified by peaks at 213, 276, 320 and 392 cm⁻¹ [22]. FeS (peaks at 492 and 293 cm⁻¹), SnS (peaks at 109, 182, 260 cm⁻¹) and Cu₂SnS₃ (peaks at 336 and 351 cm⁻¹) phases are not identified, which indicates the high phase purity of as-synthesized CFTS nanoparticles. When the amount of En is increased to 19 ml, the intensity of 320cm⁻¹ Raman peak decreases significantly, which may be caused by the small change of preferential growth direction when different amount of reaction solution is used.

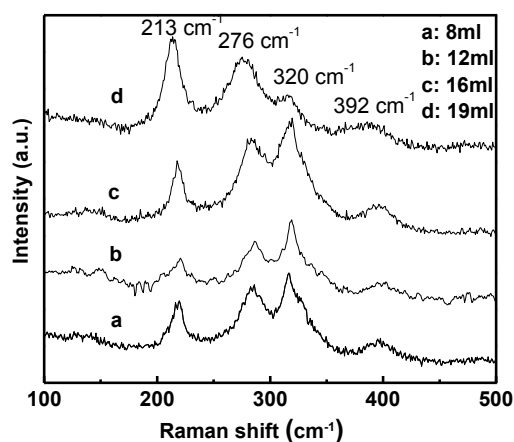


Fig. 3. Raman spectrum of the CFTS nanoparticles obtained at 220 °C for 15 hours with 8 (a), 12 (b), 16 (c), 19 (d) ml En.

The morphologies of as-synthesized CFTS nanoparticles were characterized by using SEM, as shown in Fig.4. The particle sizes of the as-synthesized CFTS nanoparticles increase with decreasing the amount of En. The formation of CFTS nanosheets is also observed at higher reaction temperatures and longer reaction times. The thicknesses of these nanosheets increase with increasing the particle sizes. In the synthesis process, metal ions and sulfur ions firstly give rise to crystal nucleus and continually grow up until the particles are formed. Larger particles may grow up by merging with smaller ones which had high surface free energy. The growth rates of different crystalline facets are not same since En molecules selectively attach to these crystalline facets. Then, some of CFTS particles may grow into platelet-like nanoparticles by oriented aggregation [23].

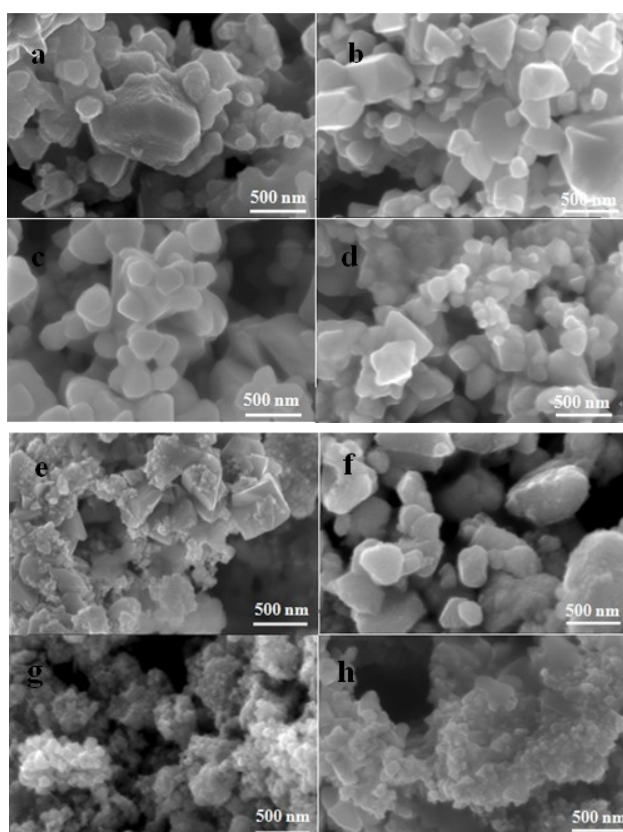


Fig. 4. SEM of CFTS nanoparticles obtained with 8 (a), 12 (b), 16 (c) and 19 (d) ml En at 220 °C for 15 hours, and with 19 ml En for 25 (e), 35 (f) hours at 220 °C, and with 19 ml En at 180 (g), 200 °C (h) for 15 hours.

The morphologies of the CFTS nanoparticles were also viewed by TEM and HRTEM, as shown in Fig.5. The average diameter of the particles are about 35 ~ 40 nm. CFTS nanoparticles synthesized with 8 ml En have bigger dimension than that synthesized with 19 ml, which agrees well with the results obtained from XRD. The crystalline structures of the CFTS nanoparticles are confirmed by the clear lattice fringes in Fig 5 (a_2, b_2). The interplanar spacing

of 3.15 Å correspond to (112) face of stannite CFTS, which agrees well with the results calculated from the diffraction peak at 28.5° in the XRD pattern. The diffraction spots in the fast Fourier transform pattern correspond to the (112), (200) and (312) planes of CFTS nanoparticles and match well with stannite CFTS.

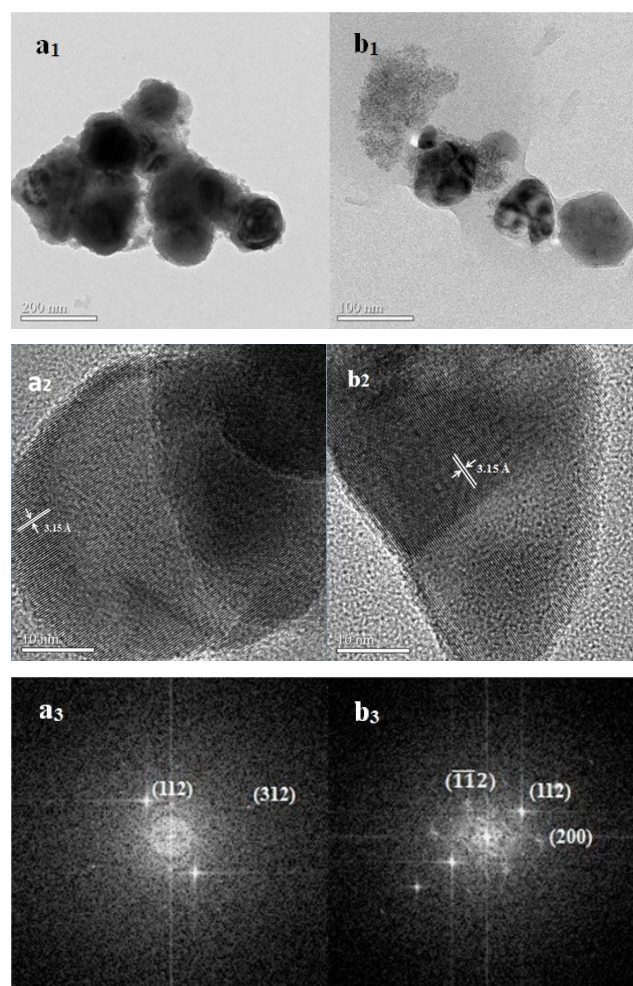


Fig. 5. TEM (a_1, b_1), HRTEM (a_2, b_2) and SAED (a_3, b_3) of CFTS nanoparticles obtained with 8 ($a_i, i = 1-3$) and 19 ($b_i, i = 1-3$) ml En.

The CFTS nanoparticles were dispersed in ethanol and the absorption spectra were measured by using liquid phase method, as shown in Fig. 6. The optical band-gaps were obtained by using the following equation [24]:

$$(\alpha h\nu)^2 = A(h\nu - E_g) \quad (6)$$

In the equation, α is the absorption coefficient, A is a constant, and E_g is the band-gap energy. By extrapolating the linear region of the plot of the absorbance squared versus energy, the band-gap energies of CFTS nanoparticles were obtained to be about 1.56 ~ 1.67 eV, as shown in the inset of Fig. 6.

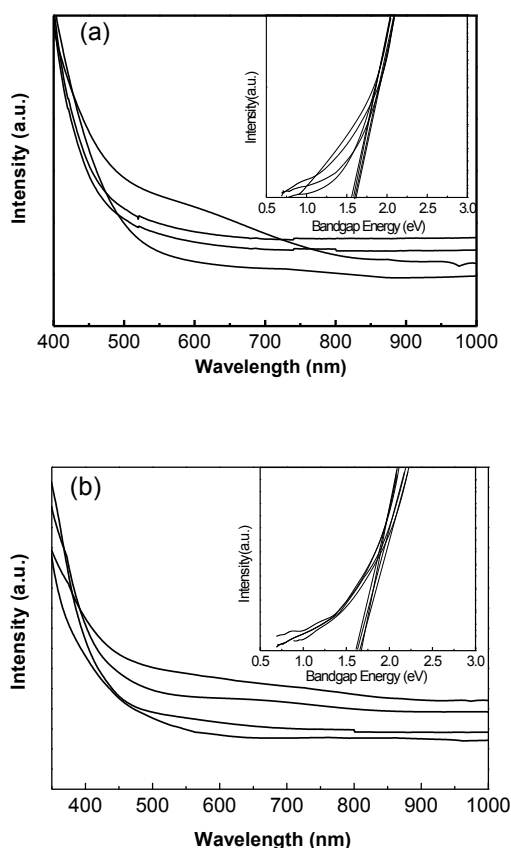


Fig. 6. The UV-Vis absorption spectra and the band-gaps (in the inset) of CFTS nanoparticles. (a): CFTS nanoparticles synthesized with 9 (a_1, a_2), 12 (b_1, b_2), 16 (c_1, c_2) and 19 ml (d_1, d_2) En at 220 °C for 15 hours. (b) CFTS nanoparticles synthesized at 180 (e_1, e_2), 200 °C (f_1, f_2) with 19 ml En for 15 hours, and with 19 ml En at 220 °C for 25 (g_1, g_2) and 35 (h_1, h_2) hours.

3.2 Performance of CFTS nanoparticle-sensitized Solar Cells

To study the photovoltaic properties of CFTS nanoparticles, CFTS nanoparticle-sensitized solar cells were fabricated and their current-voltage properties were characterized, as shown in Fig.7. The open circuit voltages are about 0.36 ~ 0.53 V and the short-circuit current densities are in the range of 0.25 ~ 0.29 mA /cm². The highest fill factor and power conversion efficiency are 59 % and 0.084 %, respectively. The power conversion efficiencies are relatively low, which can be explained as follows. Depositing p-type material in intimate contact with TiO₂ and achieving a complete conformal TiO₂ surface coverage are critical to obtaining a good quality of p-n heterojunction. As our CFTS nanoparticles are dip coated onto the TiO₂ thin films, they contact TiO₂ thin films loosely and their thicknesses are not easy to control. And cracks are also easily formed at the surface of CFTS thin films. All these may cause inefficient transfer of electrons

from the nanoparticles to TiO₂ layer. In addition, the cell structure and the device fabrication process have not been optimized. These account for the poor performance of the solar cells and the decreasing of V_{oc} , I_{sc} and power conversion efficiency with increasing the average sizes of the nanoparticles [25]. Although the efficiencies of the device demonstrated here are relatively low, possible methods to further improve the power conversion efficiencies include: (1) modifying the preparation process of TiO₂ electrode to improve the light scattering ability for light harvesting; (2) optimizing the preparation process of CFTS nanoparticle thin films to achieve a uniform coverage [26]; (3) generating a more favorable energy level alignment between CFTS nanoparticles and TiO₂ by using molecular linkers or by inserting an interfacial buffer layer [27]; (4) broadening the absorption coverage of the solar spectrum by combining alternative sensitizers in conjunction with our as-synthesized CFTS nanoparticles [28]; (5) studying new type of counter electrode material since Pt is not the ideal counter electrode for polysulphide electrolyte due to its low electro catalytic activity in polysulphide electrolyte [29].

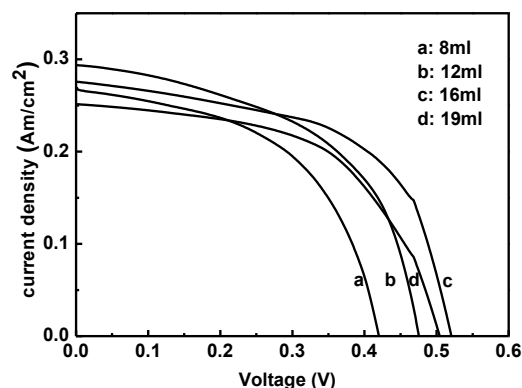


Fig. 7. Current-voltage characteristics of DSSCs based on TiO₂ photoanodes sensitized by CFTS nanoparticles obtained with 9 (a), 12 (b), 16 (c) and 19 (d) ml En at 220 °C for 15h.

4. Conclusions

CFTS nanoparticles with different morphologies have been synthesized via a low-cost solvothermal method at 180 ~ 220 °C. Morphologies and particle sizes of as-synthesized CFTS nanoparticles are greatly influenced by reaction temperatures, reaction times and the amounts of reaction solvent. CFTS nanosheets are found at longer reaction times and higher reaction temperatures. The average grain sizes of CFTS nanoparticles increase with increasing the reaction temperatures and times, and decrease with increasing the amount of the solvent. The power conversion efficiencies of CFTS nanoparticle-sensitized solar cells decrease with increasing

the average grain sizes of CFTS nanoparticles. By optimizing the cell structure and functional layers, such as buffer layers, hybrid-sensitized layers, and passivation layers, the photovoltaic performance of CFTS nanoparticle-sensitized solar cells should be enhanced.

Acknowledgements

This work was supported by the National Key Basic Research Program of China (973 program, Grant No. 2012CB934300), the National Natural Science Foundation of China (Grants No. 61006089), Shanghai City Board of Education Innovation Fund (13YZ003). We acknowledge Instrumental Analysis & Research Center of Shanghai University for the help of characterization works.

References

- [1] A.J. Clayton, S.J.C. Irvine, E.W. Jones, G. Kartopu, V. Barrioz, W.S.M. Brooks, *Sol. Energ. Mat. Sol. C.* **101**, 68 (2012).
- [2] B.A. Korevaar, R. Shuba, A. Yakimov, H. Cao, J.C. Rojo, T.R. Tolliver, *Thin Solid Films.* **519**, 7160 (2011).
- [3] H. Bi, F.Q. Huang, J. Liang, X.M. Xie, M.H. Jiang, *Adv. Mater.* **23**, 3202 (2011).
- [4] A. Wehrmann, S. Puttnins, L. Hartmann, M. Ehrhardt, P. Lorenz, K. Zimmer, *Opt. Laser Technol.* **44**, 1753 (2012).
- [5] P. Jackson, D. Hariskos, E. Lotter, S. Paetel, R. Wuerz, R. Menner, W. Wischmann, M. Powalla, *Progr. Photovolt.: Res. Appl.* **19**, 894 (2011).
- [6] D. Abou-Ras, J. Dietrich, J. Kavalakkatt, M. Nichterwitz, S.S. Schmidt, C.T. Koch, R. Caballero, J. Klaer, T. Rissom, *Sol. Energ. Mat. Sol. C.* **95**, 1452 (2011).
- [7] F.Y. Liu, Y. L.K. Zhang, B. Wang, C. Yan, Y.Q. Lai, Z. Zhang, J. Li, Y.X. Liu, *Sol. Energ. Mat. Sol. C.* **94**, 2431 (2010).
- [8] S.W. Shin, S.M. Pawar, C.Y. Park, J.H. Yun, J.H. Moon, J.H. Kim, J.Y. Lee, *Sol. Energ. Mat. Sol. C.* **95**, 3202(2011).
- [9] X.Y. Zhang, N.Z. Bao, K. Ramasamy, Y.H.A. Wang, Y.f. Wang, B.P. Lin, A. Gupta, *Chem. Commun.* **48**, 4956 (2012).
- [10] K. Woo, Y. Kim, J. Moon, *Energ. Environ. Sci.* **5**, 5340 (2012).
- [11] X.T. Lu, Z.B. Zhuang, Q. Peng, Y.D. Li, *Chem. Commun.* **47**, 3141 (2011).
- [12] Y.L. Zhou, W.H. Zhou, M. Li, Y.F. Du, S.X. Wu, *J. Phys. Chem. C* **115**, 19632 (2011).
- [13] W. Xie, X. Jiang, C.W. Zou, D. Li, J. Zhang, J. Quan, L.X. Shao, *Physica E* **45**, 16 (2012).
- [14] J.Kong, Z.J. Zhou, M.Li, W.H.Zhou, S.J. Yuan, R.Y. Yao, Y.Zhao, S.X.Wu, *Nanoscale Res. Lett.* **8**, 464 (2013).
- [15] X.K. Xin, M.He, W. Han, J.Jung, Z.Q. Lin, *Angew. Chem. Int. Ed.* **50**, 11739 (2011).
- [16] L. Shi, Q. Li, *CrystEngComm* **13**, 6507 (2011).
- [17] J. He, L. Sun, N.f. Ding, H. Kong, S.H Zuo, S.Y. Chen, Y. Chen, P.X Yang, J.H. Chu, *J. Alloy. Compd.* **529**, 34 (2012).
- [18] Q.J Guo, G.M. Ford, W.C Yang, B.C. Walker, E.A. Stach, H.W. Hillhouse, R. Agrawal, *J. Am. Chem. Soc.* **132**, 17384 (2010).
- [19] C. Yan, C. Huang, J. Yang, F.Y. Liu, J. Liu, Y.Q. Lai, J. Li, Y.X. Liu, *Chem. Commun.* **48**, 2603 (2012).
- [20] E. Thimsen, S.C. Riha, S.V. Baryshev, A.B.F. Martinson, J.W. Elam, M.J. Pellin, *Chem. Mat.* **24**, 3188 (2012).
- [21] T. Rath, W. Haas, A. Pein, R. Saf, E. Maier, B. Kunert, F. Hofer, R. Resel, G. Trimmel, *Sol. Energ. Mat. Sol. C.* **101**, 87 (2012).
- [22] C. Rincon, M. Quintero, E. Moreno, C. Power, E. Quintero, J.A. Henao, M.A. Macias, G.E. Delgado, R. Tovar, M. Morocoima, *Solid State Commun.* **151**, 947 (2011).
- [23] S.Y. Xiong, W.H. Qi, Y.J. Cheng, B.Y. Huang, M.P. Wang, Y.J. Li, *Phys. Chem. Chem. Phys.* **13**, 10648 (2011).
- [24] J.D. Servaites, B.M. Savoie, J.B. Brink, T.J. Marks, M.A. Ratner, *Ene. Environ. Sci.* **5**, 8343 (2012).
- [25] L. Li, B.L. Zhang, M. Cao, Y. Sun, J.C. Jiang, P.F. Hu, Y. Shen, L.J. Wang, *J. Alloy. Compd.* **551**, 24 (2013).
- [26] B.D. Chen, F.Z. Huang, Y.B. Cheng, R.A. Caruso, *Adv. Mater.* **21**, 2206 (2009).
- [27] S.S. Qian, C.S. Wang, W.J. Liu, Y.H. Zhu, W.J. Yao, X.H. Lu, *J. Mater. Chem.* **21**, 4945 (2011).
- [28] K.H. Lin, C.Y. Chuang, Y.Y. Lee, F.C. Li, Y.M. Chang, I.P. Liu, S.C. Chou, Y.L. Lee, *J. Phys. Chem. C* **116**, 1550 (2012).
- [29] Z. Tachan, M. Shalom, I. Hod, S. Ruhle, S. Tirosh, A. Zaban, *J. Phys. Chem. C* **115**, 6162 (2011).

*Corresponding author: caomeng@shu.edu.cn
yueshen@staff.shu.edu.cn